NUMERICAL ANALYSIS OF SHARP AEROSPIKE-INDUCED FLOW MODIFICATION FOR WAVE DRAG REDUCTION IN HYPERSONIC FLOW

Shyam Singh Kanwar[1*], Gajendra Kumar Agrawal[2], Praveen Kumar Kujur[3], Avinash Ranjan Patnaik[4], Uday Khakha[5], Sandip Kumar Sahu[6], Sharda Pratap Shrivas[7]

[1*,2,3,4,5,6]Department of Mechanical Engineering, Government Engineering College Bilaspur, Chhattisgarh, India

[7]Department of Mechanical Engineering, Chouksey Engineering College Bilaspur, Chhattisgarh, India

Corresponding Author: Shyam Singh Kanwar

Abstract

To ensure efficient design of long-duration flights, it is important to address the common issues of high surface temperature and aerodynamic drag during high-speed flights. The numerical analysis conducted for this study utilized a free stream condition of Mach 8.0, which is expected to result in turbulent flow. The aim of this study is to investigate how active and passive cooling methods synergistically reduce drag in hypersonic flight, particularly using a short spike, through numerical simulations aimed at enhancing aerodynamic efficiency and thermal management. The numerical analysis was conducted using ANSYS Fluent on a model with a 60^0 blunted cone, bluntness ratio of 0.86, cone base diameter 70 mm, and a sharp spike of different sizes located in the leading nose region. Unlike many existing studies that do not consider the turbulent model for incoming freestream flow, this investigation incorporated the k-ω turbulent model to capture turbulent phenomena. Based on the numerical results, the short spike device was found to reduce pressure drag on the forward heat shield by up to 23.78%. Utilizing a short spike in conjunction with a counter jet at a maximum pressure ratio of 43.7 resulted in a significant drag reduction of about 86.9%. This research presents an innovative technique for reducing drag in hypersonic flights through the combined use of active and passive cooling strategies. By integrating a short spike with a counter jet at a maximum pressure ratio of 43.7 that achieved a remarkable drag reduction of around 86.9%. The synergy between the passive spike and the active counter jet demonstrates significant potential for enhancing aerodynamics in high-speed flight conditions. These numerical findings suggest that the newly developed device has significant potential to serve as an effective protection heat shield for hypervelocity flight in the future.

Keywords: Hypersonic speed, pressure drag reduction, Aero-spike, ANSYS Fluent, blunted body, recirculation region

1. Introduction

The development of hypersonic flight vehicles presents a promising avenue for revolutionizing air travel and space exploration. However, significant challenges, such as high surface temperature and aerodynamic drag, must be addressed to make hypersonic flight vehicles feasible. Objects that travel at supersonic or hypersonic speeds, such as high range missiles, reusable vehicles, space shuttles, and so forth, typically have blunted cone configurations. The blunt shape configuration provides numerous advantages for high-speed travel. Firstly, it reduces aerodynamic heating by creating a shockwave that diverts the hot, compressed air away from the object, decreasing the heat load. Secondly, it reduces drag by creating a larger shockwave that diverts the high-pressure region further away from the object,

resulting in better efficiency and speed. Moreover, the blunt shape is simpler and easier to manufacture than a streamlined shape, making it a more practical option for some applications. Lastly, Maull demonstrated the blunt shape provides more volume for payload and fuel storage, making it a useful design for space vehicles [1]. One effective approach for reducing drag in hypersonic flow is through the use of aerospike devices. Aerospike devices are flow control devices designed to enhance the aerodynamic efficiency of vehicles traveling at hypersonic speeds. The design of an aerospike device includes a pointed, cone-shaped, cut shaped and spherical shaped structure that protrudes from the nose region of the vehicle. This creates a virtual spike that extends the length of the vehicle and reduces its cross-sectional area, effectively decreasing aerodynamic drag. In recent years, experimental and numerical studies have demonstrated by Sahoo *et al*, Zhong *et al* and Gerdroodbary and Hosseinalipour demonstrated the potential of aerospike devices for reducing drag and improving efficiency in hypersonic flight vehicles [2,3,4]. Flow field developed by using sharp spike as shown in figure 1.
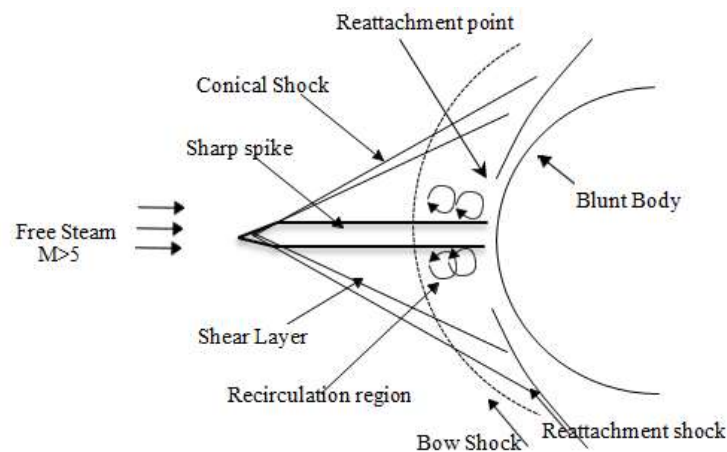

Fig.1. Flow field developed by sharp aerospike

Crawford conducted a study on a hemispherical body with sharp spikes at hypersonic Reynolds numbers ranging from 0.16×10^6 to 0.85×10^6, based on the diameter of the blunted cone body. The experimental findings indicated a significant reduction in drag and peak heat flux with the inclusion of sharp spikes of varying lengths [5]. Despite its age, this research remains a crucial point of reference for many scholars, who utilize it for validation purposes. [6,7,8,9] The impact of different spikes on a blunted body at hypersonic speeds is further discussed in the works of Mehta and Jayachandran, Menezes *et al*, Gerdroodbary *et al* and Tahani *et al*.

Researchers have extensively explored both experimental and numerical studies to delve into the significance of spike tip and aerodisk design. Gnemmi *et al* conducted a study where they analyzed three distinct aerospike designs: flat, spherical, and biconical aero disk spike. These aero disks underwent testing alongside a spike of fixed length (L/D = 1.0) and a hemisphere model. The research encompassed both experimental and numerical investigations, conducted at a Mach number of 4.5, with angles-of-attack ranging from 0° to 24° [10]. Similarly, Milichev *et al* investigated four different spike types experimentally at Mach 1.89, with a flow angle of attack of 2 degrees. Their experimental studies concluded that spikes are an effective technique for reducing wave drag [11]. Yamauchi *et al* conducted numerical investigations into various lengths of sharp spikes at Mach numbers of 2.01, 4.1, and 6.8, with flow angles of attack at 0 and 10 degrees [12]. Similarly, Huang *et al* explored the effectiveness of different lengths of flat spikes numerically at Mach 4.937, with a flow angle of attack of 0 degrees, with a flow Reynolds number of 2.2×10^7 [13]. Zhong *et al* scrutinized the impact of a flat spike on a non-

axisymmetric elliptical blunt body, noting a maximum 41% reduction in drag. They emphasized that the optimal spike length should not exceed four times the base diameter to prevent potential drag increase due to shock reattachment on the body's shoulder [3]. Sebastian *et al* carried out a numerical investigation to evaluate the impact of an aerospike on a blunt body to mitigate wave drag at Mach 6.0. They varied flow angles of attack at 0, 2, 5, and 8 degrees. Their findings emphasized that the length of the spike should not exceed four times the base diameter to prevent potential drag increase due to shock reattachment on the body's shoulder [14]. Tahani *et al* conducted a numerical study on conical, flat, and hemispherical aerospike geometries at Mach 6.0. They observed approximately a 60% reduction in drag and a 15% reduction in wall temperature [9]. The primary objective of their study was to explore the drag reduction capabilities of an aerospike device in hypersonic flow using numerical simulations. They employed the commercial CFD software ANSYS Fluent for their numerical solution [15].

2. Physical model and computational method
2.1 Physical model
In this paper, a 60-degree blunted cone is considered with a sharp spike at the nose region as shown in Fig.2. The geometry consists of two parts: the fore body and the after body. Figure 2(a) represents the 60-degree blunted cone as the fore body, and Figure 2(b) depicts the body with a sharp spike as the after body. In this study, a half-body was used for simulation to save computational time. [7] The geometry of the fore body was adopted from reference Menezes *et al*, [16] while the after body geometry was sourced from reference Ahmed *et al*.
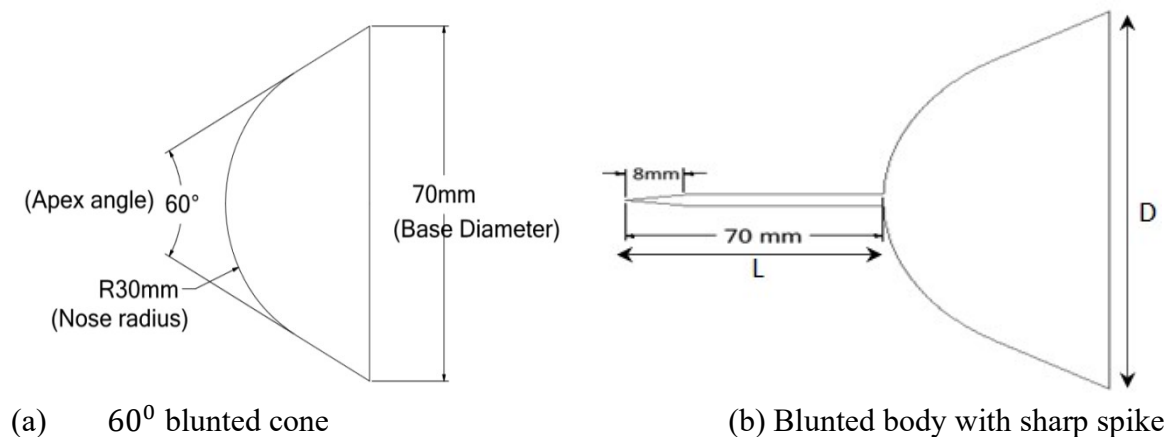

(a) 60^0 blunted cone   (b) Blunted body with sharp spike
Fig.2. the study utilized the following model geometry

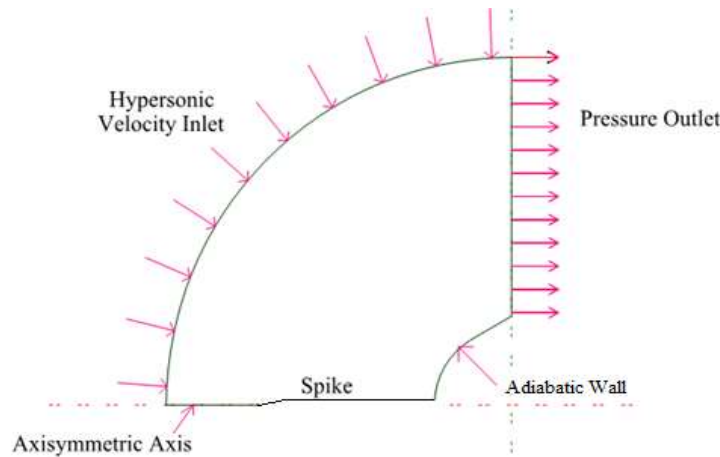### 2.2 Boundary conditions

Fig.3. Boundary conditions of computation domain

In present study, in all simulations, the initial condition for free stream consist of a inlet pressure of 219.2 Pa, air temperature of 172.4 K, and a freestream Mach number 8.0, with zero angle of attack. The boundary conditions applied to the computational domain shown in Figure 3 are as follows:

2.3 Computational grid and grid independency study

In this study, initial step involved generating a 2D axisymmetric model and computational grid utilizing the ANSYS Fluent CFD commercial software. To be precise, here utilized 106572 quad cells for situations where L/D =0.2, 68155 quad cells were used when L/D =0.5, 72,291 quad cells for L/D =0.7, 72,291 quad cells used for L/D =1.0, and 72,291 quad cell when L/D =1.5.

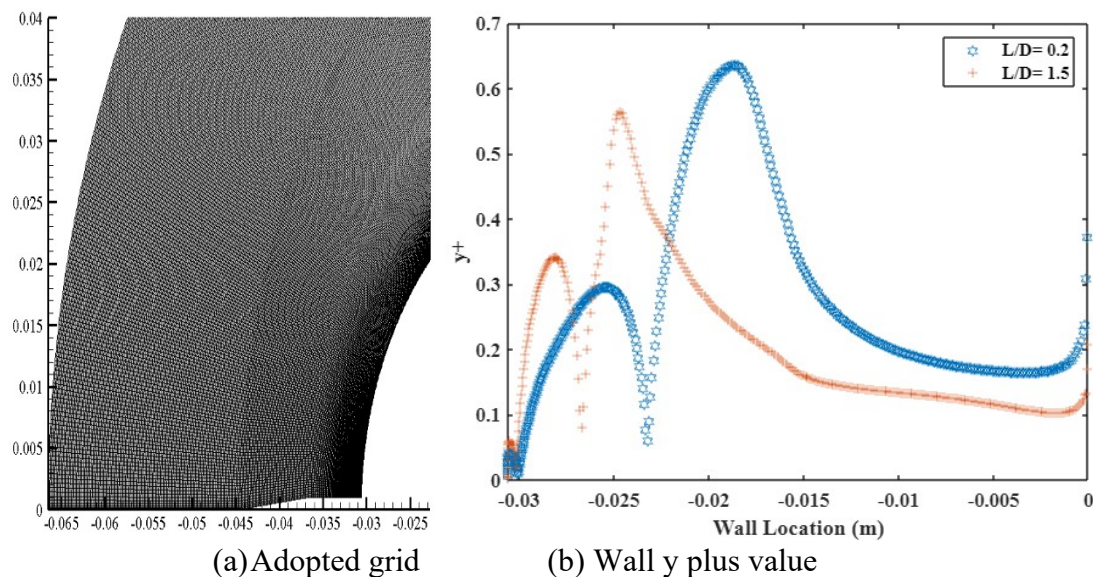(a) Adopted grid   (b) Wall y plus value
Fig. 4. The computational grid used for the simulation and wall y plus value

Figure 4(a) displays one of the computational grids employed in the simulation for L/D = 0.2. The y-plus value for the first cell near the wall was set to less than 1 to ensure proper capturing of the boundary layer. Figure 4(b) illustrates that the y-plus value near the wall surface is set to be less than 1. In the current study, a grid independence test is conducted exclusively for the "no spike" case. Grids are employed at three distinct levels: coarse, medium, and fine as shown in table 1. The findings are

displayed in Figure 5, demonstrating the solution's lack of grid dependence. By examining Figure 5, discern the Cp distribution over the blunt wall, and it becomes apparent that there is no sign of grid dependency in the simulation when the element size surpasses 62,800 as shown in figure 5.

Table 1 Grid size and maximum wall y+ value

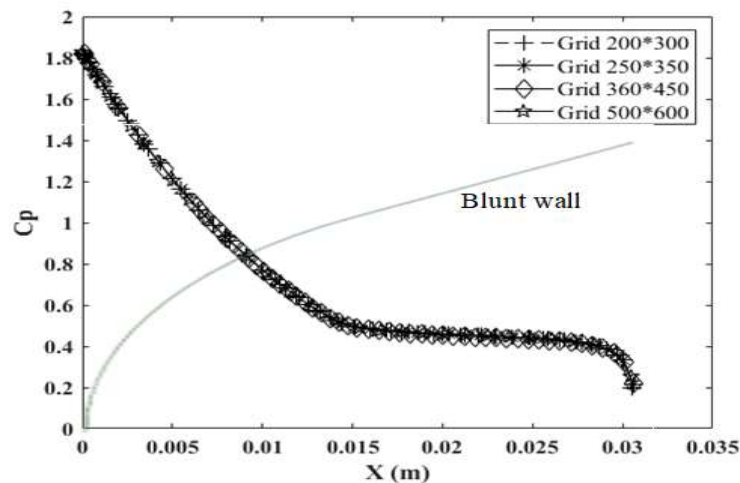| Case	Grid size	Element count	y+
Coarse	200× 300	62,800	0.3381
Medium	250× 350	70,800	0.5521
Fine	360 × 450	1,90,200	0.8683
Extra-fine	500× 600	2,91,000	0.8779

Fig 5. Grid independency study

2.4 Validation study
To validate the ANSYS setup, a no-spike case was employed. A spherical body with a 30 mm radius was utilized at Mach 8. [17] The shape of the bow shock formed in front of the object and the shock stand-off distance were compared to an empirical correlation, likely referencing by Billig. In Figure 6, the shock shape obtained from the solver closely aligns with the empirical correlation-based shape, indicating a strong agreement between the two. Moreover, the solver determined a shock standoff distance of 0.0045 meters, whereas the Billig relation predicts a standoff distance of 0.00457 meters. The close correspondence between these values suggests a reasonably good agreement between the solver results and the predictions derived from the Billig relation [17].
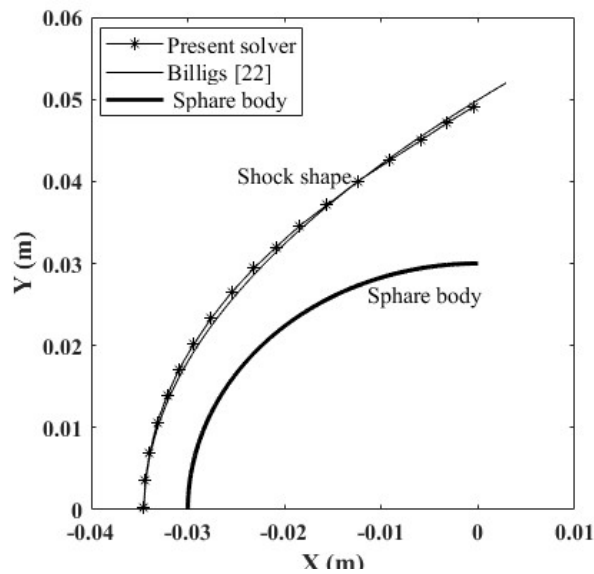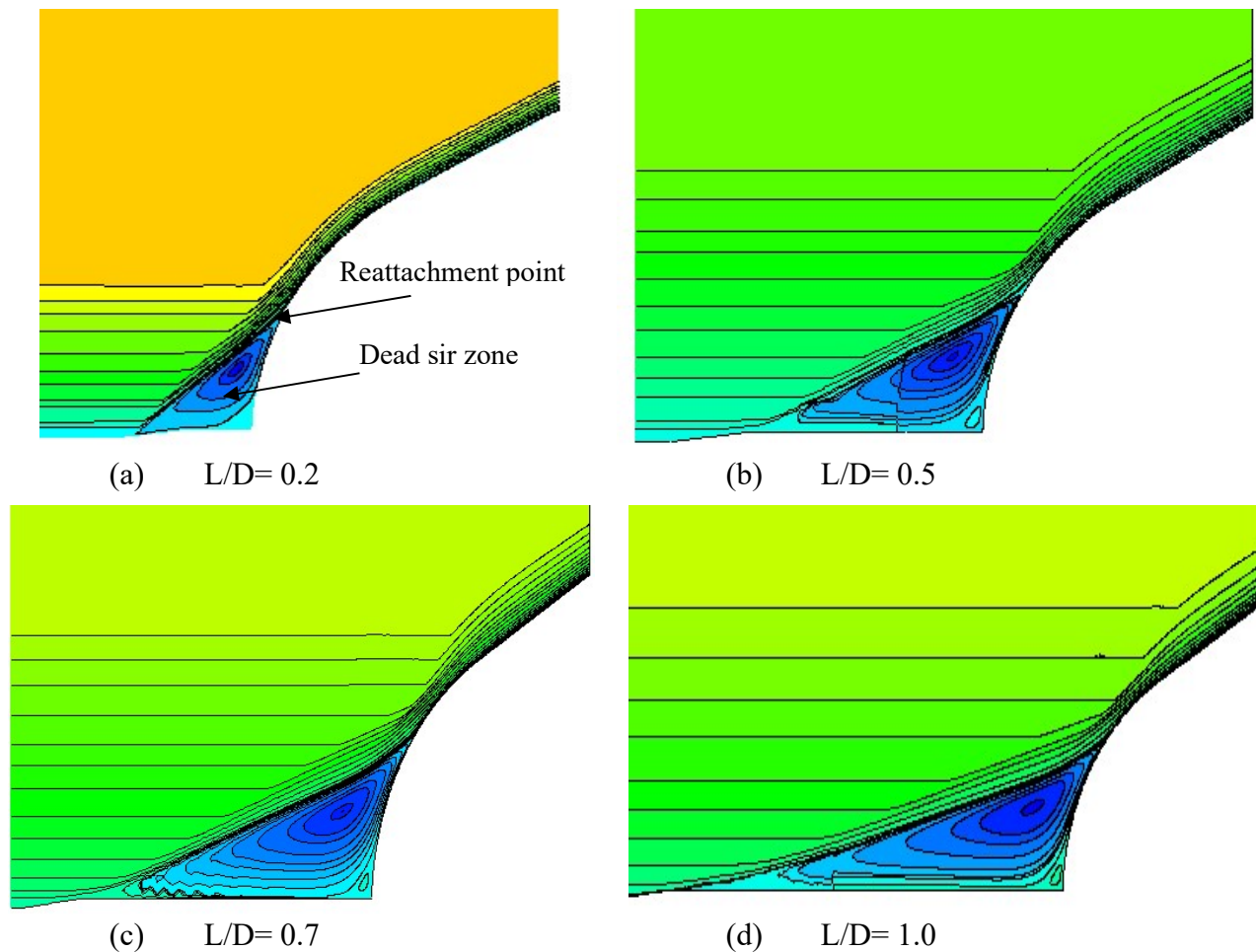
Fig 6. Comparison of shock shape

Additionally, in the present solution, drag was calculated for a 60-degree blunt cone under Mach 8 conditions. A drag coefficient of 0.839 was obtained from the solver, which was validated against Jonh *et al* results. In his result found that without the spike case, the drag coefficient was 0.844. All conditions being kept the same, there is only a 0.5% deviation observed [18]. A validation study can provide confidence that the Ansys setup can continue to be used for further simulations.

3. Result and discussion
3.1 Flow visualization around spiked blunted body
The simulation results will be presented through contours and graphs. In this simulation, the flow around the spiked body has been captured, and concurrently, the drag coefficient, representing the aerodynamic drag on the body, has been computed. Contours reveal a prominent bow shock formed around the unspiked body, resulting in significantly elevated pressure and temperature. Introducing a spike on the blunted body transforms the bow shock into a weaker conical shock. Flow separation from the spike's tip leads to the creation of recirculation regions or dead regions in front of the body, resulting in a low-pressure and low-temperature zone. This, in turn, reduces drag and lowers temperatures on the body. Mach contours are depicted in Figure 7 for various L/D ratios: 0.2, 0.5, 0.7, and 1.0. The dead air zone is clearly observable in the contour plots using streamlines.

(a)   L/D= 0.2

(b)   L/D= 0.5

(c)   L/D= 0.7

(d)   L/D= 1.0

Fig 7. Mach contours

The recirculation zone continues to increase in size as the length of the spike is extended. The reattachment point also can be observed in the Mach contours near the shoulder of the body. The expansion of the recirculation zone results in lower pressure and temperature exerted on the body.

3.2 Pressure distribution
Pressure contours can be observed from Figure 8 for L/D ratio of 0.5 and 0.7. The contours show that due to the presence of the spike, there is a reduction in pressure along the wall.
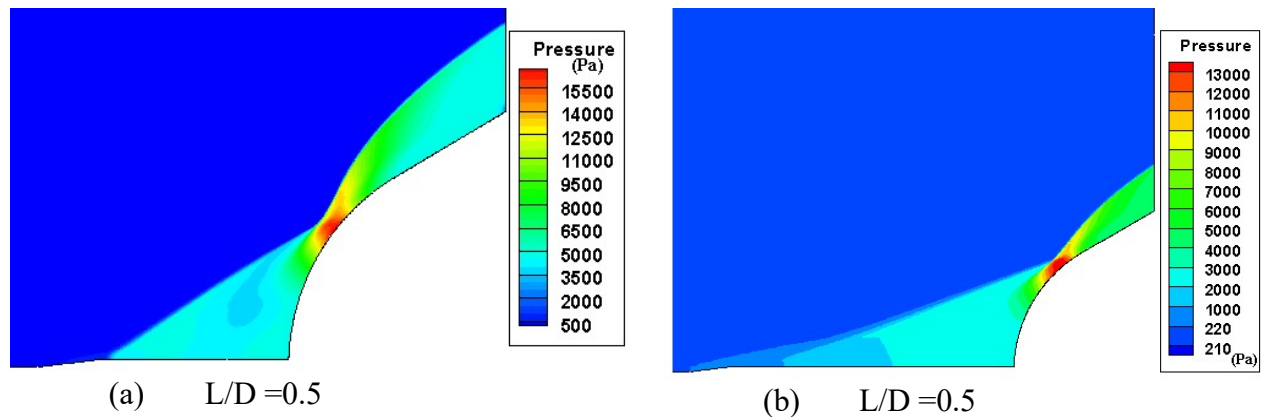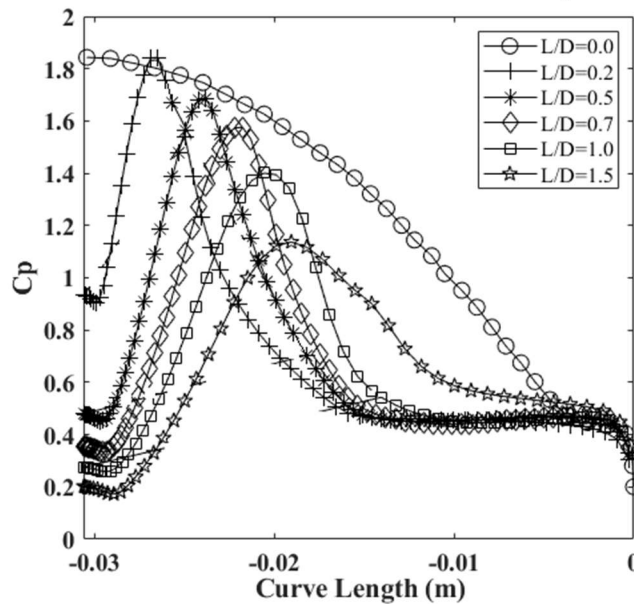
(a)   L/D =0.5   (b)   L/D =0.5

Fig. 8 Pressure contours

It can also be observed that there is a sudden increase in pressure due to shock re-compression. The pressure coefficient plot has also been calculated, and it can be seen in Figure 9 for all L/D ratios.

Fig. 9 Plot of C_p vs. wall position of sharp spike

In Figure 9, it can be observed that the wall pressure coefficient is highest for the case without a spike, maximum at the stagnation point. However, the use of the spike has resulted in not only a reduction in stagnation pressure but also an overall decrease in pressure along the entire wall. The lowest pressure at the wall is found at the maximum spike length. In addition, the use of the spike also reveals sudden pressure increases, and this is occurring due to the shock's recompression at the shoulder of the wall.

3.3 Temperature distribution
The temperature distribution over the wall is depicted in Figure 10. The temperature reaches its peak at the blunt nose cone when no aerospike is utilized, gradually decreasing along the surface of the blunt body.
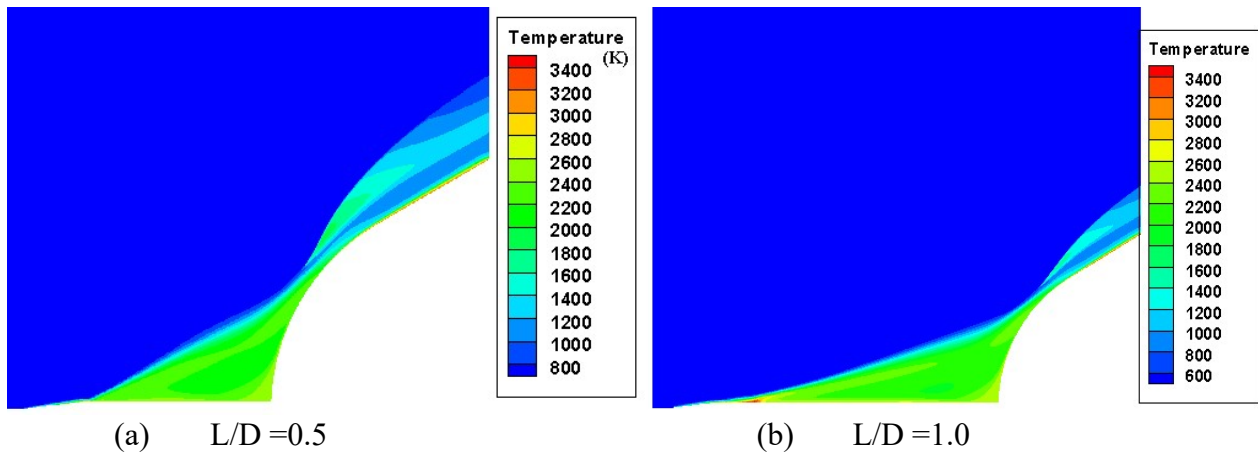
(a)   L/D =0.5   (b)   L/D =1.0

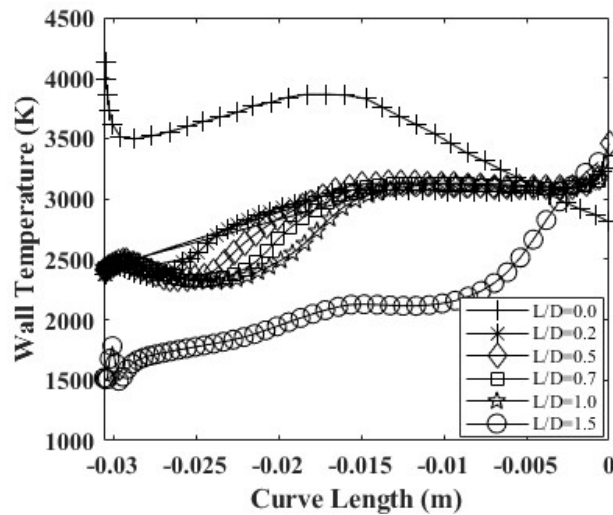**Fig. 10 Temperature Contour**

Fig. 11 Surface temperature distribution

It has been observed that the static temperature increases at the reattachment point near the vicinity of the wall for different L/D ratios.

Figure 11 shows the temperature plot for different L/D ratios. In the case without a spike, the static temperature is at its maximum, but with the use of a spike, a reduction in temperature along the wall surface can be observed.

3.4 Drag Calculation

Wave drag is typically quantified using the dimensionless drag coefficient. A coefficient of drag of 0.8383 has been evaluated for the blunt body without spike under this free stream conditions. The use of a spike has resulted in a significant drag reduction, as indicated by present simulation.

Table 2. Percentage drag reduction for different L/D ratio

L/D ratio	$y+$	C_d	% Reduction (C_d)
Spike Less	0.341	0.8383	---
0.2	0.234	0.8231	1.81 %
0.5	0.543	0.7702	8.12 %
0.7	0.342	0.7207	14.02 %

1.0	0.654	0.6788	19.02 %
1.5	0.452	0.6389	23.78 %

According to present result, a maximum drag reduction of 23.78% has been achieved at an L/D ratio of 1.5. It appears that the lowest drag was found in the smallest spike, resulting in a 1.81% reduction. The result indicates that increasing the length of the spike leads to a reduction in drag. It can be seen from Table 1 that there is very little drag reduction during a short spike. Even with a longer spike length, there is only a 23.78% drag reduction. Therefore, if you want to reduce drag using a spike, you may need to make some advancements or modifications to achieve better results. Making a short spike more effective can be achieved by injecting an opposite jet into it, which can enhance its effectiveness. In the subsequent sections, it can be clearly observed.

3.5 Drag reduction by short spike: using counter jet

Using a spike mounted on a blunt body for drag reduction is a straightforward approach. However, in the present simulation, it can be observed that using only the spike results in very minimal drag reduction with short spike. To achieve high drag reduction using a spike, a counter-jet technique can be employed in conjunction with the spiked body. Figure 12 depicts a schematic of the counter jet arrangement with the spiked body.
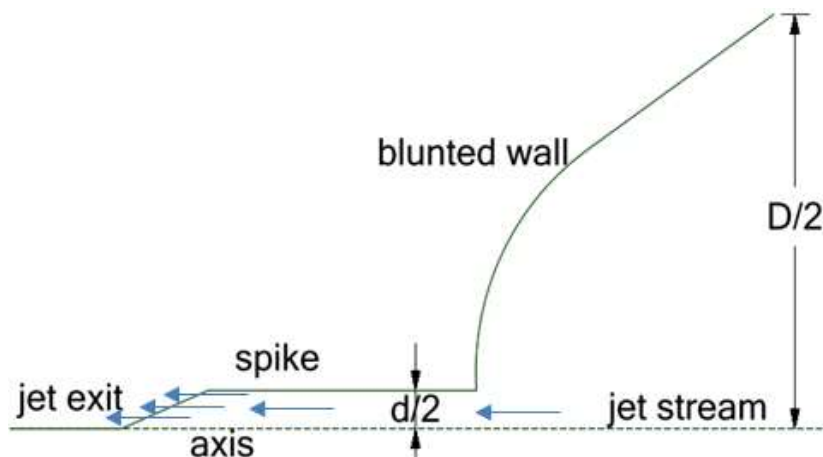

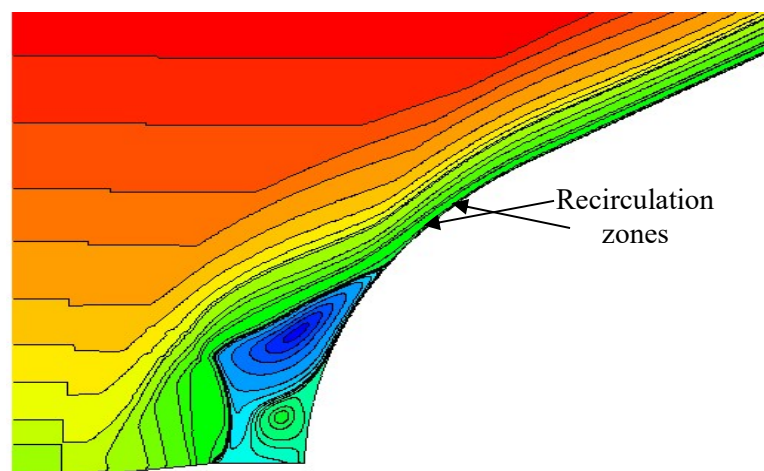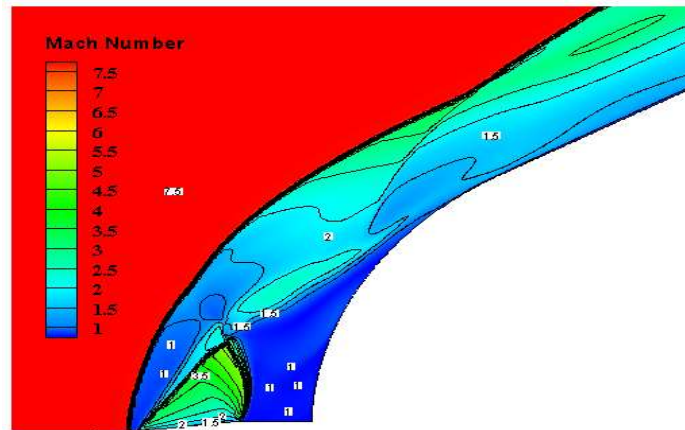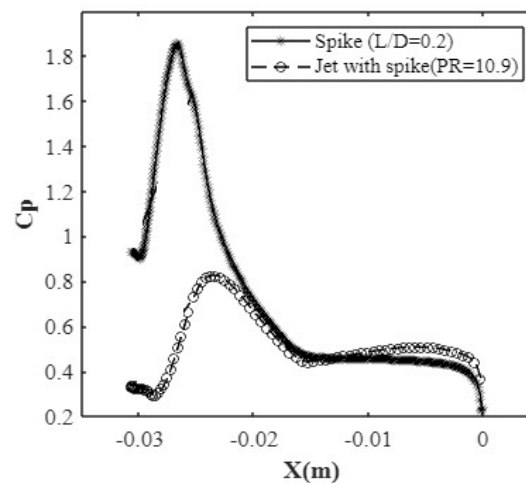**Fig. 12 Schematic of the counter jet with spike**

Fig. 13 Streamlines contours

Fig. 14 Mach contour spike with counter jet

In the current simulation, an air jet has been utilized, which emerges from the spike tip in upstream direction.

Fig. 15 Cp plot spike wit counter jet

Short spike can be used for drag reduction, especially if a counter jet is employed in it. In the current simulation, a short spike has been used with an L/D of 0.2. Injecting the jet at Mach 1 (supersonic jet) results in an air velocity of approximately 316.89 m/s, with a stagnation temperature(T_{0j}) of 300 K. Total jet pressures (P_{0j}) of 2, 4, 6, and 8 have been used to inject the air jet from the tip of spike.

The strength of the jet is determined by the pressure ratio (PR), which is the ratio of stagnation pressure of the jet (P_{0j})) to the free stream stagnation pressure ($P_{0\infty}$). Here, the pressure ratios are 10.9, 21.8, 32.8, and 43.7 for total jet pressures of 2, 4, 6, and 8 bars, respectively. This analysis shows that when a jet is injected from the spoke tip, the jet pushes the conical shock away from the body. Figure 13 illustrates that the utilization of a jet with spike results in the formation of two recirculation zones instead of one, leading to more decrease in pressure at stagnation point of body. In Figure 14, which represents the Mach contour shows, how the counter jet detaches the shock. In Figure 15, observe the comparison of the wall coefficient of pressure (Cp) between a spike and a spike with a jet.

Table 3. Percentage drag reduction for spike (L/D=0.2) with counter jet case

Pressure ratio(PR)	C_d	% Reduction
0.0	0.838	---
10.9	0.534	36.27 %
21.8	0.322	61.15 %
32.8	0.201	76.02 %
43.7	0.109	86.9 %

Through this arrangement, the total wave drag is being reduced, which can be observed in Table 3. It can be considered that using a jet with a short spike is equivalent to using a larger spike. It can be observed in the present results that at higher pressure ratios, there is an approximately 86.9% reduction in drag, even when using a short sharp spike.

4. Conclusions

A numerical simulation was conducted to reduce drag in a blunt body at Mach 8 hypersonic flow by attaching a sharp aerospike and varying the length of the aerospike. Additionally, air jets were injected from the tip of the sharp spike at different pressure ratios, and it was observed that using the jet along with the spike resulted in an improvement in drag reduction. The simulation revealed that using only the sharp spike created a recirculation region in front of the body, which contributed to drag reduction. However, due to the presence of only one recirculation region, the reduction achieved was relatively low. However, by using a counter jet in conjunction with the sharp spike, two recirculation regions are formed in front of the body. It was observed that this configuration leads to even greater drag reduction. Using only the spike, a maximum drag reduction of 23.7% was achieved at the longest spike length (L/D=1.5). However, with the shortest spike (L/D=0.2), only a 1.81% reduction in drag was observed. Indeed, a 1.81% drag reduction using only a short sharp spike might seem relatively low. From simulation it is note that with the shortest spike; only a 1.81% drag reduction was observed. This suggests that the length and shape of the spike play a crucial role in its effectiveness in reducing drag. Longer spikes may generate larger recirculation regions, leading to more significant reductions in drag, as demonstrated in the simulation. When combining a short spike with a counter jet at a pressure ratio of 43.7, a substantial reduction in drag, approximately 86.9%, was attained. Combining active and passive cooling techniques offers a promising strategy for heat management in hypersonic flight, significantly improving aerodynamic performance and thermal regulation in challenging environments. The study demonstrated that significant drag reduction can also be achieved in hypersonic flow by using a short spike.

5. References:

1. Maull DJ. Hypersonic flow over axially symmetric spiked bodies. J Fluid Mech. 1960; 8(04): 584. Available from: doi:10.1017/s0022112060000815.
2. Sahoo D, Das S, Kumar P, Prasad JK. Effect of spike on steady and unsteady flow over a blunt body at supersonic speed. Acta Astronaut. 2016; 128:521-533. Available from: doi:10.1016/j.actaastro.2016.08.005.
3. Zhong K, Yan C, Chen S, Zhang T, Lou S. Aerodisk effects on drag reduction for hypersonic blunt body with an ellipsoid nose. Aerosp Sci Technol. 2019; 86: 599-612. Available from: doi:10.1016/j.ast.2019.01.027.

4. Gerdroodbary MB, Hosseinalipour SM. Numerical simulation of hypersonic flow over highly blunted cones with spike. Acta Astronaut. 2010;67(1-2):180-193. Available from: doi:10.1016/j.actaastro.2010.01.026.

5. Crawford DH. Investigation of flow over a spiked nose hemisphere-cylinder at Mach number of 6.8. NASA-TN-D-118. 1959.

6. Mehta RC, Jayachandran T. Navier-Stokes solution for a heat shield with and without a forward facing spike. Comput Fluids. 1997;26(7):741-754. Available from: doi:10.1016/s0045-7930(97)00011-x.

7. Menezes V, Saravanan S, Reddy KPJ. Shock tunnel study of spiked aerodynamic bodies flying at hypersonic Mach numbers. Shock Waves. 2002;12(3):197-204. Available from: doi:10.1007/s00193-002-0160-3.

8. Gerdroodbary MB, Bishehsari S, Hosseinalipour SM, Sedighi K. Transient analysis of counterflowing jet over highly blunt cone in hypersonic flow. Acta Astronaut. 2012;73:38-48. Available from: doi:10.1016/j.actaastro.2011.12.011.

9. Tahani M, Karimi MS, Motlagh AM, Mirmahdian S. Numerical investigation of drag and heat reduction in hypersonic spiked blunt bodies. Heat Mass Transf. 2013;49(10):1369-1384. Available from: doi:10.1007/s00231-013-1173-4.

10. Gnemmi P, Srulijes J, Roussel K, Runne K. Flowfield around spike-tipped bodies for high attack angles at Mach 4.5. J Spacecr Rockets. 2003;40(5):622-631. Available from: doi:10.2514/2.6910.

11. Milicev, S., & Pavlovic, M. D. (2002). Influence of spike shape at supersonic flow past blunt-nosed bodies - experimental study. AIAA Journal, 40, 1018–1020. Available from: doi:10.2514/3.15157.

12. Yamauchi M, Fujii K, Higashino F. Numerical investigation of supersonic flows around a spiked blunt body. J Spacecr Rockets. 1995;32(1):32-42. Available from: doi:10.2514/3.26571.

13. Huang W, Li L, Yan L, Zhang T. Drag and heat flux reduction mechanism of blunted cone with aerodisks. Acta Astronaut. 2017;138:168-175. Available from: urldoi:10.1016/j.actaastro.2017.05.040.

14. Sebastian JJ, Suryan A, Kim HD. Numerical analysis of hypersonic flow past blunt bodies with aerospike. J Spacecr Rockets. 2016;53(4):669-677. Available from: doi:10.2514/1.a33414.

15. ANSYS Inc. Fluent User's Guide. Canonsburg, PA: ANSYS Inc.; 2012.

16. Ahmed, M. Y. M., & Qin, N. (2011). Recent advances in the Aerothermodynamics of spiked hypersonic vehicles. Progress in Aerospace Sciences, 47(6), 425–449. Available from: doi:10.1016/j.paerosci.2011.06.001.

17. Billig FS. Shock-wave shapes around spherical-and cylindrical-nosed bodies. J Spacecr Rockets. 1967;4(6):822-823. Available from: doi:10.2514/3.28969.

18. John B, Bhargava D, Punia S, Rastogi P. Drag and heat flux reduction using counterflow jet and spike - analysis of their equivalence for a blunt cone geometry at Mach 8. J Appl Fluid Mech. 2021;14(2):375-388. Available from: doi:10.47176/jafm.14.02.31648.